From quantum point contacts to quantum wires: Density-functional calculations with exchange and correlation effects

Peter Jaksch, Irina Yakimenko, and Karl-Fredrik Berggren
IFM, Linköping University, S-58183 Linköping, Sweden
(Received 22 June 2006; published 19 December 2006)

We numerically analyze the conductance and spin polarization of realistic quantum point contacts (QPCs) using density-functional theory, including both exchange and correlation effects. The self-consistent calculations are performed as a function of split gate voltage, for different temperatures and QPC lengths.We show that in short enough QPCs (100 nm) there is no spontaneous spin polarization, and the conductance for up-spin and down-spin electrons is the same. As the length of the QPC increases, so does the spin polarization and the difference in conductance between up-spin and down-spin electrons, resulting in an anomalous structure in the total conductance—the 0.7 anomaly. This structure moves from around 0.9 (in units of $2e^2/h$) for a 200 nm QPC to slightly below 0.5 for a 400 nm QPC. Due to the strong ferromagnetic spin polarization in a long QPC, it will effectively work as a spin filter. The temperature dependence of the conductance is discussed in relation to the "Reilly model," whose underlying assumption, regarding the shape of the spin gaps, is investigated using the self-consistent results.

DOI: 10.1103/PhysRevB.74.235320 PACS number(s): 73.61.−r, 71.15.Mb, 71.70.Gm

I. INTRODUCTION

The discovery of the so-called "0.7 anomaly" [1] shows how seemingly simple systems may possess remarkably rich physics, and has sparked considerable interest in the conductance properties of quantum wires and quantum point contacts (QPC). From the theory of noninteracting electrons, one expects that the conductance curve for a ballistic QPC should be quantized in steps of $2e^2/h$.[2] However, in the experimental results of Thomas *et al.*[1] there is also an additional small structure in the conductance curve around 0.7 (in units of $2e^2/h$), hence the name "0.7 anomaly." Despite its name, the 0.7 anomaly is not always pinned at 0.7 but can be observed in a range between 0.5 and 0.85 (Refs. 3–8) depending on geometry, inhomogeneities and electron density in leads. In Ref. 5, for example, there is some evidence that the value decreases with the length of the QPC (wire).

One explanation of the 0.7 anomaly, based on the idea of spontaneous ferromagnetic spin polarization driven by interactions and *ab initio* spin-density calculations, was suggested for QPC in Ref. 9, and further investigated in Refs. 10–18. Doubts have been cast on this explanation[19,20] as it would be in contradiction with the Lieb-Mattis theorem,[21] which predicts an antiferromagnetic singlet ground state. However, the Lieb-Mattis theorem only applies for strictly one-dimensional systems, in a mathematical sense, which is not the case for a typical QPC (see Ref. 22 for further discussion).

Other explanations of the 0.7 anomaly, based on Kondo-type mechanisms, have also been developed.[23–26] The unusual low-temperature behavior and the zero bias anomaly (ZBA) that have been reported for the 0.7 structure may be analyzed within such a framework. A drawback of the traditional Kondo picture is, however, that it relies on the presence of bound states, which is somewhat counterintuitive for an open system like a QPC. It has not yet been clearly explained how bound states or, at least, sharp resonances associated with quasibound states may come about for a QPC with typical device characteristics as discussed in Ref. 11. In addition, by studying the crossing of Zeeman split subbands and "0.7 analogs" Graham *et al.*[27] argue that the "Kondo-like" physics is not the root of the zero field 0.7 structure although it may enhance the conductance. In addition to the spin polarization and Kondo-type models there is at present a number of other scenarios for the 0.7 anomaly, e.g., the one-dimensional Luttinger model,[28] the formation of a Wigner lattice,[29] and effects of electron-phonon interactions.[30]

There are recent experiments that shed more light on the mechanism underlying the 0.7 structure. In particular there are three different types of experiments that favor the static spin polarization model. For example, measurements of the Fano factor reduction on the 0.7 structure have shown that it is accompanied with two conduction channels with different transmission probabilities.[31] The evolution of the reduction with parallel magnetic field B supports the picture of two channels with different spin orientations. Related studies of shot noise and dc transport in a QPC show that an observed asymmetry in noise is consistent with a phenomenological density-dependent level splitting model.[32] Most recently a half-integer plateau in a symmetric GaAs quantum wire has been observed[8] using a biased scanning probe tip. Source-drain energy spectroscopy and temperature response provide compelling evidence that the origin of the 0.5 structure is the spontaneous ferromagnetic spin polarization of the electrons in the constriction. This structure is in addition to a 0.7 structure. In general the results are sensitive to the tip position and the potential landscape. Dual conductance structures of this kind were also found in previous simulations.[10] Also most recently, Rokhinson *et al.*[33] used a spin-selective magnetic focusing technique to probe the polarization in a p-type GaAs/AlGaAs and found that static polarization is indeed present at low electron densities. Polarization is sharper in samples with a well-defined 0.7 structure, results which, according to these authors, question the Kondo interpretation.

The two different scenarios outlined above do not have to be mutually exclusive. Thus ZBA and Kondo-type features

appear to be typical for the very low temperature region [typically below a few hundred mK (Ref. 34)] and go away with a finite source-drain voltage v_{sd} and/or with magnetic field B. Spontaneous spin polarization, on the other hand, prevails at elevated temperatures, at finite v_{sd} and B. In the following we will focus on the spontaneous spin polarization and how it is driven by exchange and correlation. ZBA and Kondo-type behavior may represent interesting fundamental questions. However, spontaneous spin polarization appears more interesting in view of potential applications like spin injection and spintronics.

Focusing on spontaneous spin polarization there is the important question about the nature of the spin gap. For example, Reilly *et al.*[14–16] have developed a phenomenological model, primarily for long wires with transmission zero or one. A density-dependent spin gap is assumed to open in the one-dimensional (1D) energy spectrum each time the Fermi energy passes a subband threshold. The density dependence of the gap is assumed to be linear. Graham *et al.*, on the other hand, argue that their data give evidence that the spin gap opens abruptly[27] as predicted theoretically for infinite wires.[35,36] According to Graham *et al.* the abrupt behavior should be traced to the onset of subband fillings. In such situations, they argue, the dependence of electron density on applied gate voltage would not be linear as normally assumed. Other important questions concern geometry and the nature of the magnetized state, i.e., is it ferromagnetic, antiferromagnetic, etc.

To resolve the issues outlined above we report here on numerical modeling of typical QPC devices and their conductance and magnetic properties using the local spin-density approximation/density-functional theory (LSDA-DFT) including both exchange and correlation effects. The self-consistent calculations are performed as a function of split gate voltage, for different temperatures, and for increasing QPC lengths to explore the dependence of geometry on induced spin order, nature of spin gaps and magnetization regimes. Calculations of this type have previously been performed for shorter QPCs (see, e.g., Refs. 11 and 12). Our calculations, however, are performed also for long QPC/wires. We utilize a set of suitable basis functions that considerably reduces the computational time. By also taking the fourfold symmetry in the problem into account we are able to obtain results with very high resolution. Throughout the paper, the physics will focus on phenomena relevant to the non-ZBA/ "Kondo" regime, i.e., in which exchange correlation and spontaneous spin polarization prevails.

II. MODELING A SPLIT GATE DEVICE

We assume that the QPC is made of successive layers of GaAs, *n*-AlGaAs, and AlGaAs, where the thickness of the different layers and the doping density are the same as in Ref. 36. A metallic gate is situated on top of this structure. Depending on the geometry of the gate, different low-dimensional systems can be realized. In our case, we use the geometry in Fig. 1 in order to model the QPC. To the left and right in the figure there are two wide reservoirs with a large number of subbands occupied (around 25). Electron motion

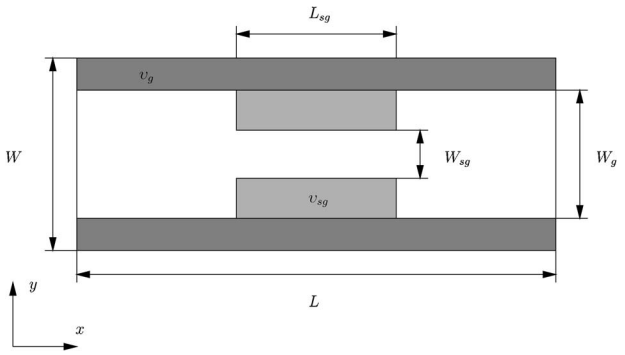

FIG. 1. Gate layout for realizing a QPC. The dark gray areas are assumed to extend to infinity in all directions leaving only the slit of width W_g. The origin is placed in the center of the constriction.

in these regions is essentially two dimensional. Between the reservoirs a narrow constriction, or channel, is formed where the electron density can be controlled by the external voltage v_{sg}. This density is very low within the parameter range we study here. In fact, there will only be a handful of electrons in the channel, which will enhance interaction effects.

We choose the direction normal to the heterostructure interface as the z axis. Assuming that confinement in this direction is much stronger than confinement in the xy plane, we may restrict ourselves to the case when only the lowest z mode is occupied, effectively rendering the problem two dimensional. The self-consistent Kohn-Sham (KS) equation then takes the form

$$\left(-\frac{\hbar^2}{2m^*}\nabla^2 + U^\sigma_{\text{eff}}(x,y)\right)\psi^\sigma_i(x,y) = \varepsilon^\sigma_i \psi^\sigma_i(x,y), \tag{1}$$

or, shorter, $H^\sigma \psi^\sigma_i(x,y) = \varepsilon^\sigma_i \psi^\sigma_i(x,y)$, where we choose the center of the constriction as the origin. The effective potential in (1) consists of electrostatic confinement, Hartree, and exchange-correlation terms

$$U^\sigma_{\text{eff}}(x,y) = U_{\text{conf}}(x,y) + U_H(x,y) + U^\sigma_{xc}(x,y). \tag{2}$$

The electrostatic confinement potential can in turn be written as a sum of different contributions

$$U_{\text{conf}}(x,y) = -eV_g(y) - eV_{sg}(x,y) - eV_d - eV_s. \tag{3}$$

Here, V_g is the potential from an infinite plane, held at voltage v_g, with a slit of width W_g; V_{sg} is the potential from the split gate that forms the QPC; the two other contributions V_d and V_s from donors and surface states can be found in Ref. 36. It is possible to derive an analytic expression for V_g (see Ref. 37)

$$V_g(y) = v_g\left\{1 - \frac{1}{\pi}\left[\arctan\left(\frac{W_g/2 - y}{z_0}\right) + \arctan\left(\frac{W_g/2 + y}{z_0}\right)\right]\right\}, \tag{4}$$

where z_0 is the vertical distance from the gate to the electron gas. To find V_{sg}, however, we use numerical integration. Including mirror charges to ensure that boundary conditions are satisfied we get

$$V_{sg}(x,y) = \int \frac{v_{sg} z_0}{2\pi[z_0^2 + (x-x')^2 + (y-y')^2]^{3/2}} dx'dy', \quad (5)$$

where the integration is performed over the surface of the split gate, held at potential v_{sg}. The Hartree term U_H in (2) is calculated in a similar fashion,

$$U_H(x,y) = \frac{e^2}{4\pi\epsilon\epsilon_0} \int \rho(x',y') \left(\frac{1}{\sqrt{(x-x')^2 + (y-y')^2}} - \frac{1}{\sqrt{(x-x')^2 + (y-y')^2 + 4z_0^2}} \right) dx'dy'. \quad (6)$$

Here, the second term stems from the mirror charges. Integration is performed over the whole computational area. For the important exchange-correlation potential U_{xc}, finally, we use the parametrization from Refs. 38 and 39. Although not stated explicitly, in order to break the (spin) symmetry of the problem, we also add a Zeeman term, associated with a weak in-plane magnetic field in the x direction. In the iterative scheme for solving the KS equation we let this term be present only in the first iteration.

We solve the KS-LSDA equations for the geometry in Fig. 1 using periodic boundary conditions. However, rather than solving the equation directly by discretization on a grid, we introduce a set of basis functions. This procedure will reduce the size of the problem. In the x direction the system is open, which makes a basis set consisting of plane waves suitable. The number of these lateral basis functions depends on several parameters, e.g., the length L_{sg} and width W_{sg} of the constriction. Typically, we use between 30 and 50 of them. In the y direction the system is closed, and the transverse modes are well described by a basis set consisting of Gaussian functions, in particular in the QPC region in which the confinement is closed to parabolic in y^2. In our case, around 40 of them are required in order to provide accurate results.We have checked this approach by comparing with numerical integration of the transverse wave functions in infinite wires with multisubbands occupied.[36]

More explicitly, the lateral basis functions have the form

$$\phi_m(x) = \frac{1}{\sqrt{L}} e^{ik_m x}, \quad (7)$$

where $k_m = 2\pi m/L$. The transverse Gaussian basis functions are chosen as eigenfunctions of the harmonic oscillator,

$$\varphi_n(y) = \sqrt{\frac{\alpha}{\sqrt{\pi} 2^{n-1}(n-1)!}} e^{-\alpha^2 y^2/2} H_{n-1}(y), \quad (8)$$

where H_{n-1} is the Hermite polynomial of order $n-1$, and the parameter α is of the same order of magnitude as the width W_{sg} of the channel. To improve the quality of the basis set α can be tuned empirically.

The basis functions for the two-dimensional (2D) problem are tensor products of the functions in (7) and (8). An arbitrary KS orbital ψ_i can be expanded in a linear combination according to

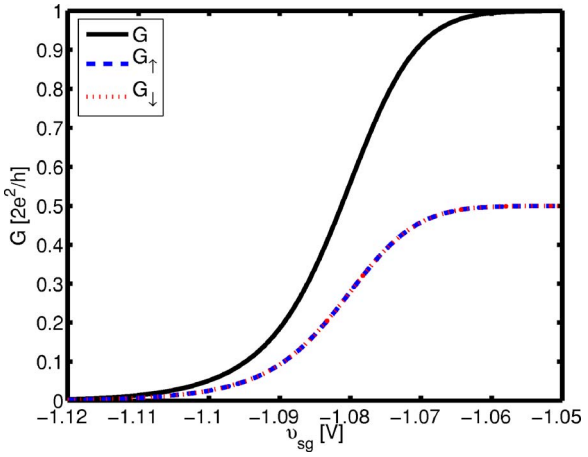

FIG. 2. (Color online) Conductance as a function of split gate voltage for a 100 nm QPC.

$$\psi_i(x,y) = \sum_{m,n}^{M,N} c_{mni} \phi_m(x) \otimes \varphi_n(y), \quad (9)$$

where c_{mni} are the expansion coefficients. For ease of notation we label the basis functions χ_j, using a single index defined as $j=(m-1)N+n$. Multiplying Eq. (1) from the left by a specific $\chi_{j'}(x,y)$ followed by integration yields

$$\sum_j c_{ji} \langle \chi_{j'} | H | \chi_j \rangle = \varepsilon_i \sum_j c_{ji} \langle \chi_{j'} | \chi_j \rangle. \quad (10)$$

Note that since we have chosen the basis functions to become orthogonal the term $\langle \chi_{j'} | \chi_j \rangle$ in (10) simplifies to $\delta_{j'j}$. Repeated use of the above procedure leads to a matrix eigenvalue problem

$$\mathbf{HC} = \mathbf{C}\boldsymbol{\varepsilon},$$

$$H_{j'j} = \langle \chi_{j'} | H | \chi_j \rangle, \quad (11)$$

where $\boldsymbol{\varepsilon}$ is a diagonal matrix containing the values ε_i. Normally, the matrices in (11) will not be sparse so a direct

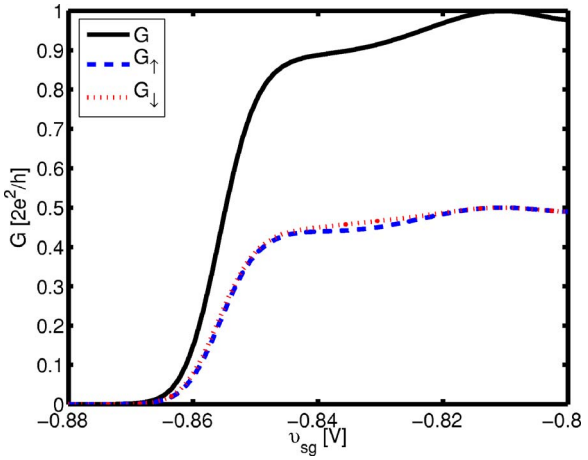

FIG. 3. (Color online) Conductance as a function of split gate voltage for a 200 nm QPC.

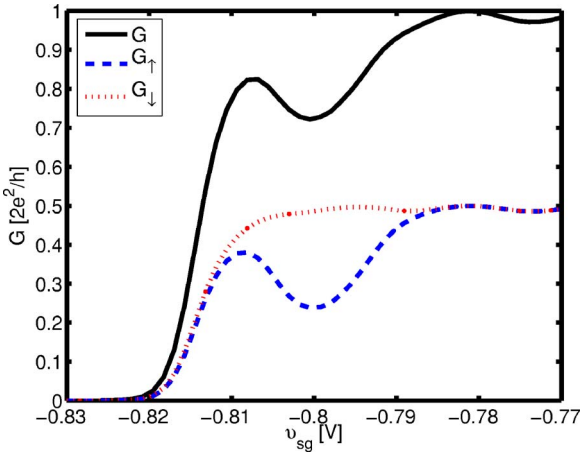

FIG. 4. (Color online) Conductance as a function of split gate voltage for a 250 nm QPC.

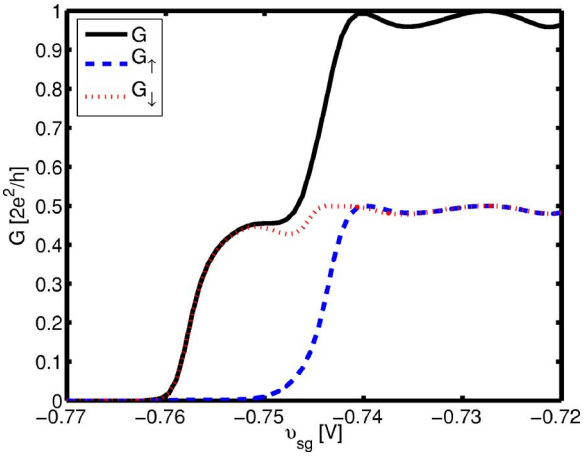

FIG. 6. (Color online) Conductance as a function of split gate voltage for a 400 nm QPC.

approach for calculating eigenvalues and eigenvectors must be applied. The great advantage here is that the dimension of **H** is typically considerably smaller than that of the matrix obtained when discretizing H directly on a grid.

The solution of (11) is used to calculate the electron density, which is in turn used to update the effective potential (2) from which a new electron density can be obtained. The procedure is repeated until a self-consistent solution is reached. We use the effective potential from this solution to calculate the conductance through the QPC. For a source-drain bias v_{sd} the differential conductance is given by the expression

$$G = \frac{2e^2}{h} \sum_n \int_{-\infty}^{\infty} T_n(E) \frac{\partial}{\partial v_{sd}} [f(E,\mu_L) - f(E,\mu_R)] dE, \quad (12)$$

where the sum runs over the occupied subbands; $f(E,\mu) = 1/\{\exp[(E-\mu)/k_BT)]+1\}$ is the Fermi-Dirac distribution for temperature T and chemical potential μ. Here $\mu_{L,R} = E_f \pm e v_{sd}/2$ for left and right reservoirs assuming a symmetric potential drop; T_n are the transmission coefficients for the different modes which are calculated for open boundary conditions with continuous matching of wave functions and their derivatives. At small source-drain bias and zero temperature, expression (12) simplifies to the Landauer-Büttiker formula[2]

$$G = \frac{2e^2}{h} \sum_n T_n(E_f), \quad (13)$$

III. RESULTS

We calculate electron and spin densities as well as conductance, as described in the preceding section, for the parameter choice: $v_g = -0.73$ V, $W = 420$ nm, $W_g = 400$ nm, $W_{sg} = 80$ nm, $L = 800$ nm; L_{sg} is varied from 100 nm up to 400 nm; v_{sg} is chosen to display the first step in the conductance curve.

The first set of calculations is performed for zero temperature and varying L_{sg}. For the case of $L_{sg} = 100$ nm, i.e., a short constriction, the conductance curves are similar for up-spin ($G_\uparrow$) and down-spin ($G_\downarrow$) electrons (Fig. 2). But as L_{sg} increases, the difference in conductance becomes pronounced (Figs. 3–6). In these figures also the total conduc-

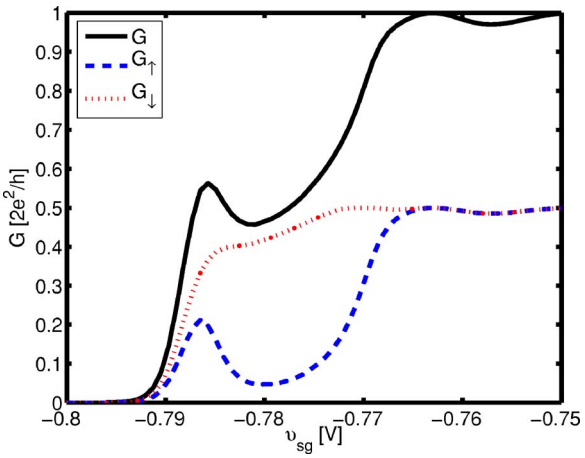

FIG. 5. (Color online) Conductance as a function of split gate voltage for a 300 nm QPC.

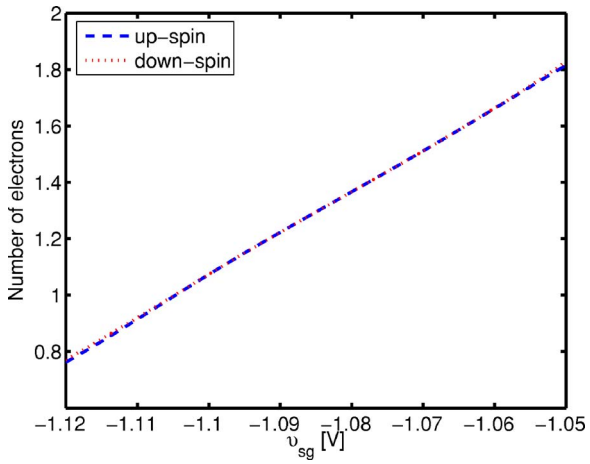

FIG. 7. (Color online) The number of up- and down-spin electrons in a 100 nm QPC as a function of the split gate voltage.

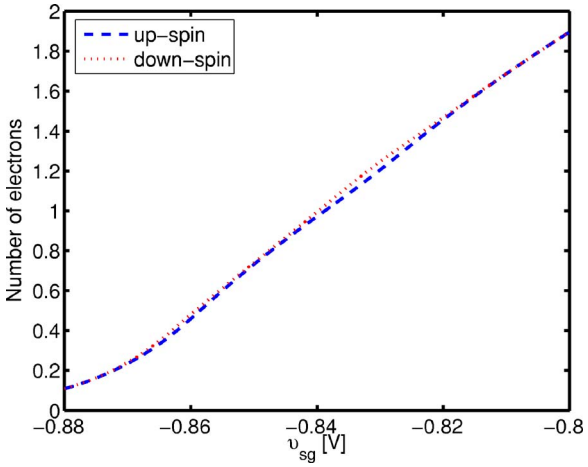

FIG. 8. (Color online) The number of up- and down-spin electrons in a 200 nm QPC as a function of the split gate voltage.

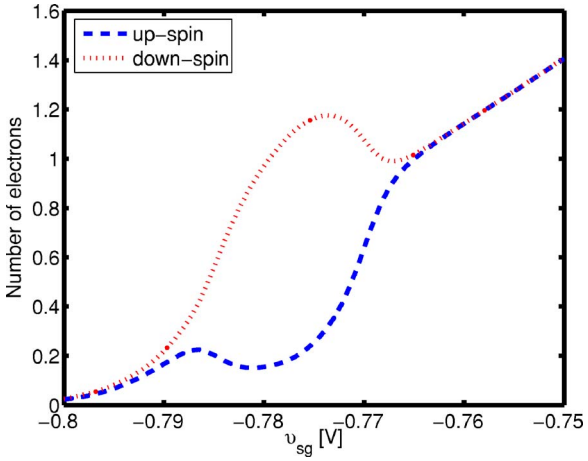

FIG. 10. (Color online) The number of up- and down-spin electrons in a 300 nm QPC as a function of the split gate voltage.

tance G is plotted. It is clearly seen that when $G_\uparrow$ and $G_\downarrow$ differ, there is an anomalous structure in G that evolves from around 0.9 (Fig. 3) to slightly below 0.5 (Fig. 6). The oscillations around 1.0 in the total conductance, and the peak in the anomalous structure, are likely to be caused by some kind of broad resonance depending on the gate geometry. Our results are in good qualitative agreement with experiments,[3–6] and also with theoretical results.[11,12,40] However, we remark that due to differences in gate layout, heterostructure, donor density, theoretical modeling, etc., the results should not be compared quantitatively. Also, experimental results obtained for long QPCs are sensitive to accidental constrictions and other disorder effects caused by, e.g., impurities and inhomogeneities.[41,42]

For a measure of the spin polarization, we calculate the number of up- and down-spin electrons in the interior of the QPC, as a function of v_{sg}, for the different choices of L_{sg} (see Figs. 7–11). For $L_{sg}=100$ nm the number of electrons is essentially the same for both spin directions over the whole range of voltages (see Fig. 7), and there is no spontaneous spin polarization; in the other cases the voltage interval, for which ferromagnetic polarization occurs, agrees well with the interval where the conductance for up- and down-spin electrons differs. Evidently, for a short wire/QPC there is in practice no magnetization. With increasing length magnetization clearly sets in and grows in magnitude. Another observation is that the total number of electrons in the split gate region is basically a linear function of the gate voltage, i.e., our results do not support the abrupt filling of subbands as proposed by Graham *et al.*[27]

We remark that the conductance properties of the system with $L_{sg}=400$ nm are close to those expected for a long ideal quantum wire; the up-spin conductance stays flat at 0 while the down-spin conductance reaches almost 0.5. The transmission coefficients are to a first approximation either zero or one as expected for long wires. An interesting observation of practical value is that this system works as a spin filter and could, in principle, be used for spin injection.

In Fig. 12 we have plotted the effective potentials in the 400 nm QPC, along the cross section $y=0$, for a fixed gate voltage. For polarized down-spin electrons there is a dip in the effective potential inside the QPC. One might suspect that this potential could contain narrow quasibound states, supporting the Kondo picture. However, there is no sign of

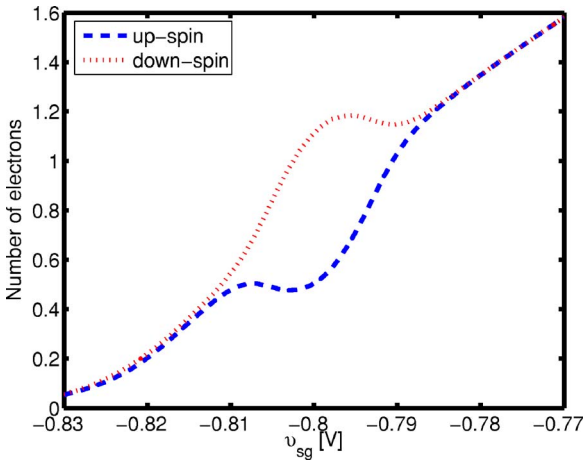

FIG. 9. (Color online) The number of up- and down-spin electrons in a 250 nm QPC as a function of the split gate voltage.

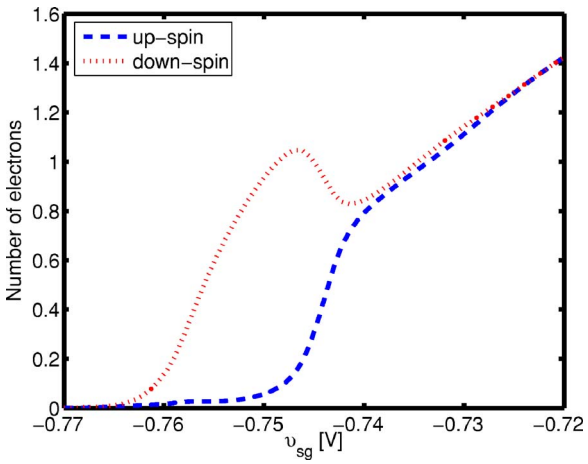

FIG. 11. (Color online) The number of up- and down-spin electrons in a 400 nm QPC as a function of the split gate voltage.

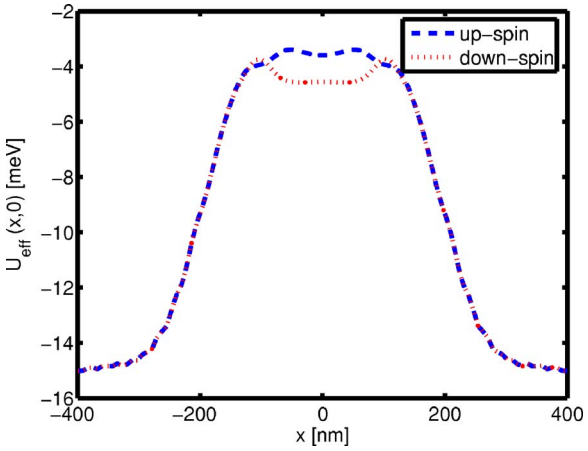

FIG. 12. (Color online) The effective potential, for v_{sg}= −0.75 V, for up- and down-spin electrons along the cross section y=0 in a 400 nm QPC.

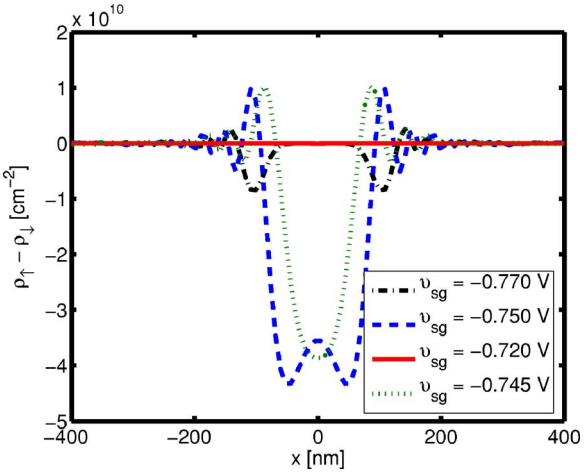

FIG. 14. (Color online) The difference between up- and down-spin electron densities along the cross section y=0 in a 400 nm QPC.

such states in the total electron density (plotted along y=0 in Fig. 13); neither are there any resonances in the corresponding conductance curve (Fig. 6).

At low densities, electrons inside a long QPC are predicted to form a Wigner crystal with an antiferromagnetic ground state.[43] Calculations, based on both standard LSDA and exact configuration interaction methods for finite closed wires and rings also suggest the presence of charge modulation at low densities, referred to as "Wigner molecules" because of finite size.[44,45] However, in Fig. 13 no density modulations can be observed, and Fig. 14, displaying the difference in up- and down-spin electron density along y=0, shows that the spin state is still of ferromagnetic type. We have also performed calculations where we have relaxed the assumption that spins are only directed along the z axis, to allow for noncollinear spins. However, these calculations did not change the overall features of Figs. 13 and 14. Hence, we draw the conclusion that, for device parameters used here, neither the formation of a Wigner crystal lattice nor an antiferromagnetic ground state will be observed for our long 400 nm wire. For the shorter wires, 250 and 300 nm, the spin gap closes at finite conduction. In that regime the polarization splits spatially into two parts.[10] On further decrease of the voltage these two parts move to opposite ends of the QPC and aquire antiparallel spin ordering. Hence the total magnetization is zero as in Figs. 9 and 10.

We now turn to the issue of temperature dependence by repeating the above conductance calculations for T=0, 1, 2, and 3 K. For the short 100 nm and 200 nm QPC our model is not able to replicate the experimental results[1,3,34,46] showing that the anomaly becomes more pronounced with increasing temperature. In our case, we only observe temperature smearing of the conductance curves (not shown in the paper); there is no sign of any distinct anomaly. However, for the longer 250 nm and 300 nm QPCs the agreement with experiments[5] is much better. These results are summarized in Figs. 15 and 16. In the former case the anomalous structure evolves from around 0.75 down to around 0.65 with increasing temperature; in the latter case the anomaly moves in the

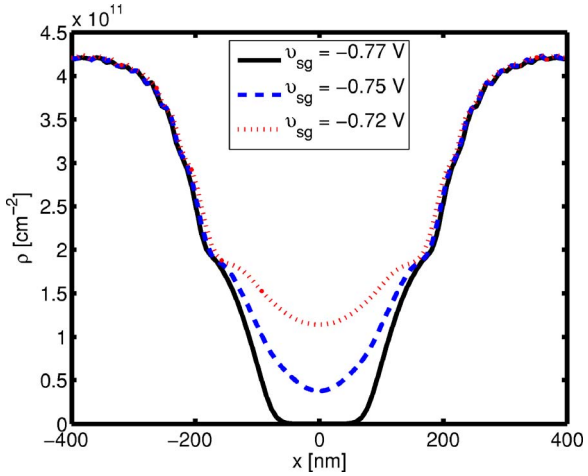

FIG. 13. (Color online) The total electron density along the cross section y=0 in a 400 nm QPC.

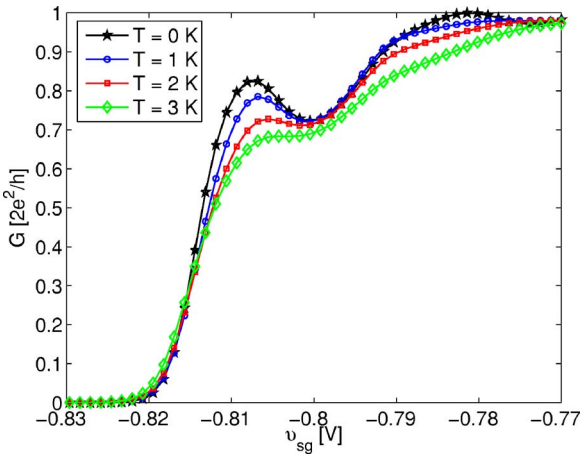

FIG. 15. (Color online) Conductance as a function of split gate voltage for different temperatures in a 250 nm QPC.

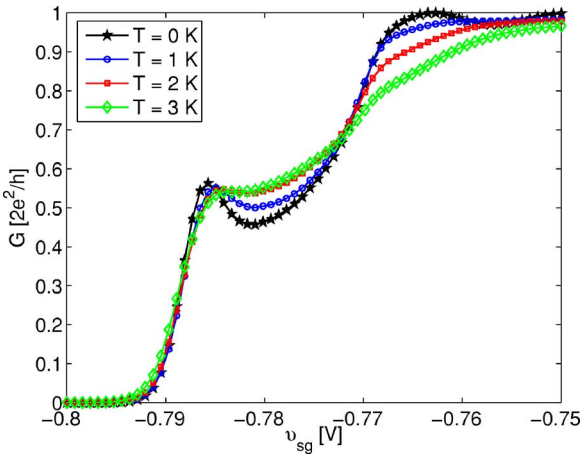

FIG. 16. (Color online) Conductance as a function of split gate voltage for different temperatures in a 300 nm QPC.

opposite direction, starting from around 0.50 and evolving up to around 0.55. In both cases increasing temperature makes the conductance curves smoother. The overall features are similar in shape to those calculated theoretically in. Ref. 12.

The temperature dependence of the conductance can be explained by the "Reilly model," [15] which is based on an assumption of a spin gap that opens linearly as a function of the 1D electron density inside the QPC. This model can be seen as an extension of the one developed by Kristensen *et al.*,[46] in that it gives a specific form for the spin gap. To examine the validity of the assumption of a linear spin gap we calculate the energy difference between the lowest subband E_1 in the QPC and the effective potential U_{eff} at $x=y=0$, as a function of the one-dimensional electron density ρ_{1D} at $x=y=0$, for up- and down-spin electrons. Results for the 250, 300, and 400 nm QPCs are shown in Figs. 17–19, respectively. As the lowest down-spin subband starts to populate, Hartree interaction causes its energy to increase [in relation to $U_{\text{eff}}(0,0)$]. Also, a spin gap will open between the up- and down-spin subband as a consequence of exchange

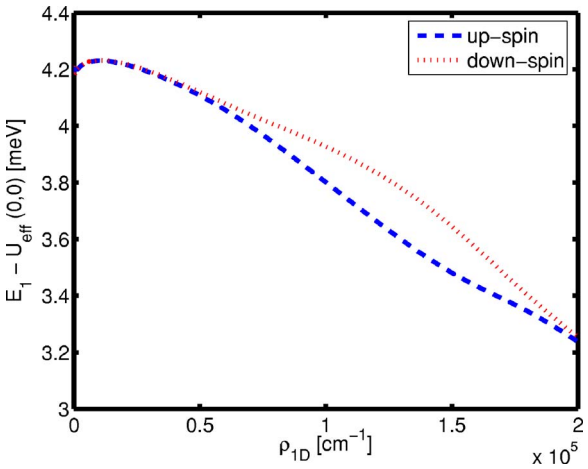

FIG. 17. (Color online) The energy difference between the lowest subband and the effective potential at $x=y=0$, as a function of the one-dimensional electron density, in a 250 nm QPC.

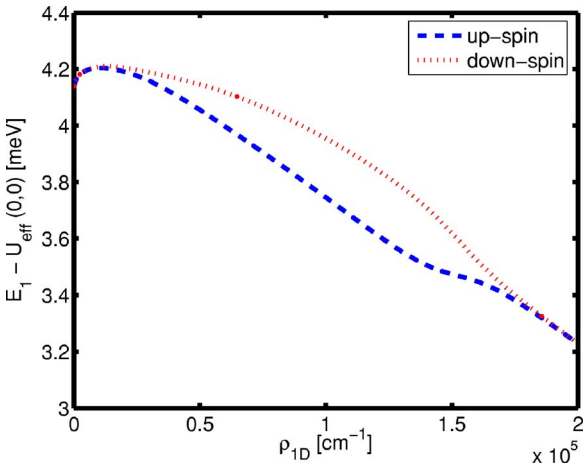

FIG. 18. (Color online) The energy difference between the lowest subband and the effective potential at $x=y=0$, as a function of the one-dimensional electron density, in a 300 nm QPC.

interaction. As seen in the figure, the opening process can be described, at least piecewise, by a linear approximation. However, as the voltage increases the spin gap starts to close again. Although not shown in the figure we mention that the spin gap will open again for each new subband that populates, although smaller for each time. This behavior is not incorporated in Reilly's model and it is not clear how it will affect the overall conclusions that can be drawn from the model.

Ignoring the reservation above, with the terminology in Ref. 15 the temperature dependence in Fig. 15 is explained by a slowly opening spin gap, whereas in Fig. 16 the spin gap opens rapidly, cf. the first figure in Ref. 15. This is in agreement with our results in Figs. 17 and 18.

IV. SUMMARY

We have used the Kohn-Sham local spin-density equations to study the transport, spontaneous magnetization, spin

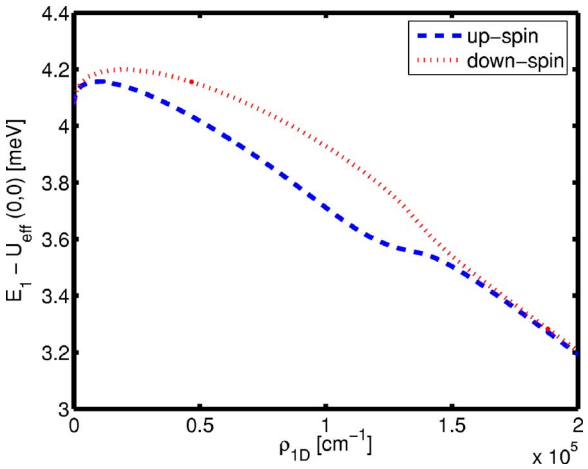

FIG. 19. (Color online) The energy difference between the lowest subband and the effective potential at $x=y=0$, as a function of the one-dimensional electron density, in a 400 nm QPC.

gaps and spin order in some typical ballistic semiconductor split-gate devices. The theory is approximate but appears to catch basic features such as local spin polarization induced by electron interactions. For example, when compared with more accurate methods like configuration interaction[44] for quantum dots it turns out that the local density technique yields a spin correlation function which agrees quite well with the more accurate methods.

We have found that spontaneous ferromagnetic spin polarization is capable of explaining the conductance anomaly in long QPCs. Moreover, we have discovered that long QPCs could have applications for the purpose of spin injection. We have also partly justified the assumption of a linear opening of the spin gaps in the Reilly model, with the important addition that also the closing of the spin gaps should be incorporated in the model.

Note added in proof. Recently, Rejec and Meir[47] have also shown how different spin-polarized states may be formed. Thus, symmetric and antisymmetric spin polarization close to pinch-off, as reported briefly in this paper, are also discussed by Rejec and Meir in detail.

ACKNOWLEDGMENTS

The authors are grateful to A. Graham, K.J. Thomas, M. Pepper, D. Reilly, and S. Reimann for fruitful discussions and helpful comments and J. Henriksson for generous help with the graphics. The authors acknowledge general support from I. Abrikosov, and financial support from The Swedish Research Council. The authors have also benefited from collaboration within the European COLLECT project.

[1] K. J. Thomas, J. T. Nicholls, M. Y. Simmons, M. Pepper, D. R. Mace, and D. A. Ritchie, Phys. Rev. Lett. **77**, 135 (1996).
[2] M. Büttiker, Phys. Rev. B **41**, 7906 (1990).
[3] C.-T. Liang, M. Pepper, M. Y. Simmons, C. G. Smith, and D. A. Ritchie, Phys. Rev. B **61**, 9952 (2000).
[4] K. S. Pyshkin, C. J. B. Ford, R. H. Harrell, M. Pepper, E. H. Linfield, and D. A. Ritchie, Phys. Rev. B **62**, 15842 (2000).
[5] D. J. Reilly, G. R. Facer, A. S. Dzurak, B. E. Kane, R. G. Clark, P. J. Stiles, J. L. O'Brien, N. E. Lumpkin, L. N. Pfeiffer, and K. W. West, Phys. Rev. B **63**, 121311(R) (2001).
[6] A. Ghosh, C. J. B. Ford, M. Pepper, H. E. Beere, and D. A. Ritchie, Phys. Rev. Lett. **92**, 116601 (2004).
[7] N. T. Bagraev, I. A. Shelykh, V. K. Ivanov, and L. E. Klyachkin, Phys. Rev. B **70**, 155315 (2004).
[8] R. Crook, J. Prance, K. J. Thomas, S. J. Chorley, I. Farrer, D. A. Ritchie, M. Pepper, and C. G. Smith, Science **312**, 1359 (2006).
[9] C.-K. Wang and K.-F. Berggren, Phys. Rev. B **54**, R14257 (1996).
[10] K.-F. Berggren and I. I. Yakimenko, Phys. Rev. B **66**, 085323 (2002).
[11] A. A. Starikov, I. I. Yakimenko, and K.-F. Berggren, Phys. Rev. B **67**, 235319 (2003).
[12] P. Havu, M. J. Puska, R. M. Nieminen, and V. Havu, Phys. Rev. B **70**, 233308 (2004).
[13] P. S. Cornaglia, C. A. Balseiro, and M. Avignon, Phys. Rev. B **71**, 024432 (2005).
[14] D. J. Reilly, T. M. Buchler, J. L. O'Brien, A. R. Hamilton, A. S. Dzurak, R. G. Clark, B. E. Kane, L. N. Pfeiffer, and K. W. West, Phys. Rev. Lett. **89**, 246801 (2002).
[15] D. J. Reilly, Phys. Rev. B **72**, 033309 (2005).
[16] D. J. Reilly, Y. Zhang, and L. DiCarlo, Physica E Proc. EPS-16 (2005).
[17] A. Ashok, R. Akis, D. Vasileska, and D. K. Ferry, Mol. Simul. **31**, 797 (2005).
[18] F. Malet, M. Pi, M. Barranco, and E. Lipparini, Phys. Rev. B **72**, 205326 (2006).
[19] R. Fitzgerald, Phys. Today **55**, 21 (2002).
[20] J. R. Minkel, Phys. Rev. Focus **10**, 24 (2002).
[21] E. Lieb and D. Mattis, Phys. Rev. **125**, 164 (1962).
[22] P. Jaksch, K.-F. Berggren, and I. I. Yakimenko, Nanotechnology **16**, 1924 (2005).
[23] P. E. Lindelof, Proc. SPIE **4415**, 77 (2001).
[24] Y. Meir, K. Hirose, and N. S. Wingreen, Phys. Rev. Lett. **89**, 196802 (2002).
[25] K. Hirose, Y. Meir, and N. S. Wingreen, Phys. Rev. Lett. **90**, 026804 (2003).
[26] T. Rejec, A. Ramsak, and J. H. Jefferson, Phys. Rev. B **67**, 075311 (2003).
[27] A. C. Graham, M. Pepper, M. Y. Simmons, and D. A. Ritchie, Phys. Rev. B **72**, 193305 (2005).
[28] L. Bartosch, M. Kollar, and P. Kopietz, Phys. Rev. B **67**, 092403 (2003).
[29] K. A. Matveev, Phys. Rev. Lett. **92**, 106801 (2004).
[30] G. Seelig and K. A. Matveev, Phys. Rev. Lett. **90**, 176804 (2003).
[31] P. Roche, J. Ségala, D. C. Glattli, J. T. Nicholls, M. Pepper, A. C. Graham, K. J. Thomas, M. Y. Simmons, and D. A. Ritchie, Phys. Rev. Lett. **93**, 116602 (2004).
[32] L. DiCarlo, Y. Zhang, D. T. McClure, DJ. Reilly, C. M. Marcus, L. N. Pfeiffer, and K. W. West, Phys. Rev. Lett. **97**, 036810 (2006).
[33] L. P. Rokhinson, L. N. Pfeiffer, and K. W. West, Phys. Rev. Lett. **96**, 156602 (2006).
[34] S. M. Cronenwett, H. J. Lynch, D. Goldhaber-Gordon, L. P. Kouwenhoven, C. M. Marcus, K. Hirose, N. S. Wingreen, and V. Umansky, Phys. Rev. Lett. **88**, 226805 (2002).
[35] C.-K. Wang and K.-F. Berggren, Phys. Rev. B **54**, R14257 (1996).
[36] K.-F. Berggren, P. Jaksch, and I. Yakimenko, Phys. Rev. B **71**, 115303 (2005).
[37] J. Martorell, H. Wu, and D. W. L. Sprung, Phys. Rev. B **50**, 17298 (1994).
[38] C. Attaccalite, S. Moroni, P. Gori-Giorgi, and G. B. Bachelet, Phys. Rev. Lett. **88**, 256601 (2002).
[39] C. Attaccalite, S. Moroni, P. Gori-Giorgi, and G. B. Bachelet, Phys. Rev. Lett. **91**, 109902(E) (2003).
[40] O. P. Sushkov, Phys. Rev. B **64**, 155319 (2001).
[41] A. A. Starikov, I. I. Yakimenko, K.-F. Berggren, A. C. Graham, K. J. Thomas, M. Pepper, and M. Y. Simmons, Proc. SPIE **5023**,

267 (2002).
[42] K. Gloos, P. Utko, M. Aagesen, C. B. Sørenson, J. B. Hansen, and P. E. Lindelof, Phys. Rev. B **73**, 125326 (2006).
[43] A. D. Klironomos, J. S. Meyer, and K. A. Matveev, Europhys. Lett. **74**, 679 (2006).
[44] M. Borgh, M. Toreblad, M. Koskinen, M. Manninen, S. Aberg, and S. M. Reimann, Int. J. Quantum Chem. **817**, 105 (2005).
[45] S. M. Reimann and M. Manninen, Rev. Mod. Phys. **74**, 1283 (2002).
[46] A. Kristensen, H. Bruus, A. E. Hansen, J. B. Jensen, P. E. Lindelof, C. J. Marckmann, J. Nygard, C. B. Sorensen, F. Beuscher, A. Forchel, and M. Michel, Phys. Rev. B **62**, 10950 (2000).
[47] T. Rejec and Y. Meir, Nature (London) **442**, 900 (2006).